SCIENTIFIC REPORTS
nature research

Check for updates

OPEN

Fractionation of carbon and hydrogen isotopes of TSR-altered gas products under closed system pyrolysis

Quanyou Liu[1,2]✉, Weilong Peng[1,2], Qingqiang Meng[1,2], Dongya Zhu[1,2], Zhijun Jin[1,2] & Xiaoqi Wu[1,2]

Thermochemical sulfate reduction (TSR) is common in marine carbonate gas reservoirs, leading to complicated isotope characteristics of TSR-altered gas. This study aims to better understand how TSR affects the geochemical and isotopic compositions of alkanes in pyrolysis products. Pyrolysis of TSR were conducted with crude oil, nonane (C_9) and methylnaphthalene (MN) in the presence of $MgSO_4$ solution at temperatures of 350 °C, 360 °C, and 370 °C for different durations of 4–219 h in a closed system. Results show that carbon and hydrogen isotope compositions of alkane gas resulting from TSR (pyrolysis with crude oil and $MgSO_4$) became heavier with increasing carbon number, i.e., $\delta^{13}C_1 < \delta^{13}C_2 < \delta^{13}C_3$ and $\delta^2H\text{–}C_1 < \delta^2H\text{–}C_2 < \delta^2H\text{–}C_3$. Compared with the $\delta^{13}C_1$, $\delta^{13}C_2$ and $\delta^{13}C_3$ increased in a much wider range as heating continued. Carbon and hydrogen isotopes of alkane gas produced by TSR became heavier with increasing gas souring index. Values for $\delta^{13}C_1\text{–}\delta^{13}C_2$ and $\delta^2H\text{–}C_1\text{–}\delta^2H\text{–}C_2$ typically decreased as oil and C_9 underwent thermal cracking. Comparative experiments using C_9 in the presence of $MgSO_4$ produced partially reversed carbon isotope series ($\delta^{13}C_1 > \delta^{13}C_2$), which, for the first time, confirmed the ability of TSR to cause isotopic reversal from pyrolysis. The residual heavy alkanes gradually became ^{13}C-enriched during TSR, which increased $\delta^{13}C_2$ values and changed the partially reversed isotope sequence to a positive sequence ($\delta^{13}C_1 < \delta^{13}C_2$). The discovery of a partial reversal of the carbon isotope series of alkane gases through pyrolysis will further deepen the understanding of TSR-altered natural gas.

H_2S is a harmful gas usually generated in deep marine carbonate gas reservoirs[1–6], which poses significant challenges for the safe production of natural gas. High concentrations of H_2S in gas reservoirs are mainly produced by thermochemical sulfate reduction (TSR)[1,7–11], during which sulfate is reduced by organic matters and/or hydrocarbons to H_2S and CO_2. In general, hydrocarbons with higher carbon number will react more readily with sulfate[12–14]. The reaction equations can be expressed as follows:

$$SO_4^{2-} + CH_4 \rightarrow CO_3^{2-} + H_2S + 2H_2O$$

$$3SO_4^{2-} + 4C_2H_6 \rightarrow CO_3^{2-} + 3H_2S + 4CH_4 + CO_2 + H_2O$$

$$3SO_4^{2-} + 2C_3H_8 \rightarrow 3CO_3^{2-} + 3H_2S + 2CH_4 + CO_2 + H_2O$$

$$3SO_4^{2-} + 4C_4H_{10} + H_2O \rightarrow 5CO_3^{2-} + 5H_2S + 8CH_4 + 3CO_2$$

The effect of TSR has been studied extensively by characterising natural gas components, stable isotopes such as carbon, hydrogen, and sulfur, as well as inclusions and sulfur-bearing minerals[9,15–30]. Cai et al.[23,24] concluded

[1]State Key Laboratory of Shale Oil and Gas Enrichment Mechanisms and Effective Development, SINOPEC, Beijing 100083, China. [2]Petroleum Exploration and Production Research Institute, SINOPEC, Beijing 100083, China. ✉email: qyouliu@sohu.com

that CH_4 can be oxidised when the dryness coefficient is greater than 0.97 and presented fractionation equations for TSR in the presence of methane and ethane[27,28]. Machel et al.[4] proposed an initiation temperature of 100–140 °C for TSR, and Worden et al.[31] thought that the initiation temperature for TSR was 140 °C. Amrani et al.[29] and Meshoulam et al.[32]systematically investigated the isotopic composition of sulfur compounds during TSR and proposed that the composition of sulfur isotopes may reflect the degree of TSR. Hao et al.[1,] Liu et al.[20,21], and Cai et al.[27] characterised geochemical properties of marine gas in the Sichuan Basin, China, and found that heavy hydrocarbons were preferentially involved in the TSR reaction compared with CH_4, which can increase the dryness coefficient of natural gas. TSR was also found to gradually cause partial carbon isotope reversal of the positive alkane gas series[20]. Liu et al.[21] discovered that hydrogen isotope fractionation for CH_4 generated by TSR via hydrogen isotope exchange between water and hydrocarbons was greater than that for CH_4 directly generated from kerogen. Although a carbon isotope fractionation model for alkane gas in H_2S-bearing gas reservoirs, such as the commonly observed pattern of the carbon isotope series of CH_4 and C_2H_6 that changes from positive to reversed and then back to positive[1,20,33], has been established, the hydrogen isotope fractionation of alkane gas has not been explored by laboratory pyrolysis. Liu et al.[34] proposed that the rock salt and/or brine may play an important role for the occurrence of TSR based on the formation mechanism of H_2S-enriched gas reservoirs in the Sichuan Basin, China. Cross et al.[35] reported, based on laboratory simulations, that temperature was the key factor for the occurrence of TSR, whereas pressure had a minor impact. Pan et al.[12] conducted a high-temperature, long-time, step-by-step thermal cracking simulation with organic matter and Fe_2O_3, $MgSO_4$, and a mixture of both. They found that CH_4 was produced by TSR in the presence of heavy hydrocarbons and that isotope fractionation became more pronounced with increasing carbon number. Based on a thermal cracking simulation, Zhang et al.[36,37] proposed that the initiation temperature for TSR was affected by the chemical composition of crude oil, and low molar ratios of water and $MgSO_4$ were favorable to the reaction. $MgSO_4$ affects pH, which in turn increases the concentration of the active sulfate species HSO_4^-[38,39]. TSR eventually oxidised CH_4 into carbon dioxide[19–21]. Zhao et al.[40] experimentally simulated the TSR reaction with crude oil, bitumen, and different kinds of kerogen under presence of anhydrite and $MgSO_4$, and found that TSR preferentially modified low molecular hydrocarbons, and type III kerogen was least reactive during the TSR process.

However, most of these laboratory simulations of TSR have focused on the chemical composition, and carbon isotope composition of the pyrolysis[12,36–41]. The effects of oil cracking and TSR on the hydrogen isotopic composition of alkane gas have rarely been studied[42]. In addition, participation of water in the reaction and involvement of hydrogen from other sources, e.g. water, can result in a hydrogen isotope fractionation of alkane gas that may differ from its carbon isotope fractionation[21].

In this paper, crude oil, nonane (C_9H_{20}, C_9), and methylnaphthalene ($C_{11}H_{10}$, MN) were used to simulate TSR alteration at different thermal stages. The chemical and carbon isotopic composition of gaseous products from thermal cracking and TSR of crude oil were analysed to elucidate the impact of TSR. In addition, this is the first study that considered the impact of the presence of water during TSR alteration on the hydrogen isotope fractionation of alkane gas. Therefore, the effects of thermal cracking and TSR on the fractionation of carbon and hydrogen isotopes of alkane gas were studied to explore the isotopic evolution of carbon and hydrogen caused by TSR, aiming to provide experimental evidence to better understand the isotopic composition and variation of gases in H_2S-bearing reservoirs.

Methods

Samples. Crude oil sample used in the simulation experiments were collected from the TK772 well within the Ordovician Yingshan Formation ($O_{1-2}y$) in the No.7 District of the Tahe Oilfield, Tarim Basin, western China, at a depth of 5,557.5–5,591.5 m. The content of saturated hydrocarbons, aromatic hydrocarbons, non-hydrocarbons, asphaltene, and sulfur of the crude oil were measured as 25.28%, 28.66%, 12.23%, 17.26%, and 2.46%, respectively, with a carbon isotope composition of − 32.8‰ (the hydrogen isotopic composition was not measured). The purities of C_9 (C_9H_{20}, nonane) and MN ($C_{11}H_{10}$, methylnaphthalene) were 99.99%. The reaction reagents and experimental buffer in this paper were manufactured by the Aladdin Reagent Shanghai Co., Ltd.

Experimental procedures and product analyses. It has been reported that the most suitable temperature for TSR of crude oil in a closed system is approximately 360 °C and that heating time and pH are important factors affecting the occurrence of TSR[10,36]. To simulate the evolution of reaction products during thermal cracking and TSR, as well as the change in isotopic composition caused by TSR, crude oil samples were heated at a temperature of 360 °C for 4, 10, 24, 40, 72, and 219 h. For each condition, the experiment was conducted with crude oil only, and a mixture of crude oil, buffer and $MgSO_4$. In the pyrolysis system, we added a mixed salt solution (including 5.61 g $MgCl_2$, 10.01 g NaCl and 100 ml distilled water, 350 mg solution per gold capsule) to the gold capsule. A mixture of silica and talc (1:1, about 60 mg per gold capsule) was used as a buffer to maintain a relatively stable pH of approximately 3–5. To determine the effects of temperature on TSR, experiments were also conducted using a solution of crude oil, buffer, and $MgSO_4$ at temperatures of 350 °C and 370 °C. For each experiment, about 10 mg of crude oil, $MgSO_4$ solution, and buffer were combined in a gold capsule (60 mm in length, 6 mm in diameter) under argon gas. The gold capsules were placed in different autoclaves that were connected to each other. The pressure of the experimental system was maintained at 50 MPa to simulate the conditions under which most TSR occurs. After the reaction temperature was increased from room temperature (18 °C) to 200 °C at a rate of 20 °C/h, it was kept constant at 200 °C for half an hour to stabilise the system temperature. The temperature was then increased to the target temperature at a rate of 20 °C/h, and held constant for the pre-set reaction time. The gold capsules were then taken out of the autoclaves and quenched. Fluctuations of temperature and pressure in the autoclaves were 0.5 °C and 1 MPa, respectively. To compare and analyse the

Reaction condition	No	Time (h)	Easy-Ro (%)	Yield of main products (ml/g)								Chemical composition of main products (%)							C_1/C_{1-5} (%)
				CH_4	C_2H_6	C_3H_8	C_4H_{10}	C_5H_{12}	H_2	CO_2	H_2S	CH_4	C_2H_6	C_3H_8	C_4H_{10}	C_5H_{12}	CO_2	H_2S	
360 °C oil	M-8	4	0.80	1	0.36	0.23	0.08	0.01	0.06	0.75	–	39.84	14.31	9.11	3.25	0.49	29.83	n.d	59.46
	M-9	10	0.90	3.53	1.45	1.05	0.46	0.1	0.23	0.98	–	45.1	18.53	13.39	5.92	1.29	12.52	n.d	53.54
	M-10	24	1.00	8.2	3.47	2.52	1.18	0.3	0.25	1.39	–	47.33	20.02	14.54	6.8	1.71	8	n.d	52.36
	M-11	40	1.10	14.47	6.27	4.86	2.71	0.93	0.28	1.92	–	46.01	19.92	15.44	8.62	2.95	6.1	n.d	49.51
	M-12	72	1.19	24.06	10.08	7.66	4.25	1.52	0.3	1.99	0.22	48.02	20.12	15.28	8.48	3.04	3.97	0.43	50.58
	M-13	219	1.40	38.09	16.07	13.14	8.27	3.59	0.5	2.51	1.08	45.75	19.3	15.79	9.93	4.31	3.01	1.29	48.12
360 °C oil + $MgSO_4$ + buffer	M-15	4	0.80	9.94	2.76	2.1	0.94	0.29	0.23	41.38	47.92	9.41	2.61	1.99	0.89	0.28	39.19	45.38	61.99
	M-16	10	0.90	27.75	6.41	2.5	0.74	0.2	0.17	35.24	131.95	13.54	3.13	1.22	0.36	0.1	17.19	64.38	73.79
	M-17	24	1.00	34.71	4.04	0.3	0.1	0.03	0.14	112.59	308.11	7.55	0.88	0.07	0.02	0.01	24.47	66.98	88.51
	M-18	40	1.10	38.17	1.54	0.08	0.02	–	0.15	135.34	357.66	7.16	0.29	0.02	n.d	n.d	25.39	67.11	95.85
	M-19	72	1.19	40.52	0.18	0.01	–	–	0.12	179.99	378.63	6.76	0.03	n.d	n.d	n.d	30.03	63.16	99.56
	M-20	219	1.40	34.32	0.03	–	–	–	0.14	190.38	307.6	6.44	0.01	n.d	n.d	n.d	35.75	57.77	99.84
350 °C oil + $MgSO_4$ + buffer	M-31	7.5	0.80	0.99	0.26	0.17	0.07	0.04	0.05	15.02	2.33	5.23	1.37	0.88	0.37	0.21	79.3	12.32	64.89
	M-32	19.5	0.90	9.03	1.83	1.11	0.33	0.09	0.09	29.67	47.46	10.08	2.05	1.24	0.37	0.1	33.11	52.96	72.83
	M-33	42	1.00	23.91	6.52	2.75	0.59	0.08	0.1	158.03	420.05	3.91	1.06	0.45	0.1	0.01	25.82	68.63	70.71
	M-34	79.5	1.10	35.35	7.23	3.11	0.43	0.02	0.08	193.52	487.53	4.86	0.99	0.43	0.06	n.d	26.61	67.03	76.66
	M-35	172	1.23	37.04	2.89	0.08	0.03	–	0.07	201.12	546.65	4.7	0.37	0.01	n.d	n.d	25.53	69.38	92.52
360 °C oil + $MgSO_4$ + buffer	M-36	4	0.80	1.05	0.28	0.16	0.05	0.01	0.07	11.69	0.31	7.71	2.05	1.2	0.37	0.08	85.68	2.29	67.57
	M-37	10	0.90	7.21	1.38	0.79	0.2	0.05	0.16	20.22	32.07	11.61	2.22	1.27	0.32	0.08	32.57	51.66	74.90
	M-38	24	1.00	26.31	5.52	2.47	0.57	0.09	0.2	188.31	373.92	4.4	0.92	0.41	0.1	0.02	31.52	62.59	75.21
	M-39	40	1.10	37.19	7.8	2.41	0.55	0.09	0.16	246.62	512.89	4.6	0.97	0.3	0.07	0.01	30.53	63.5	77.31
	M-40	72	1.19	42.29	4.6	0.14	0.03	–	0.06	277.72	626.79	4.44	0.48	0.01	n.d	n.d	29.18	65.86	90.06
370 °C oil + $MgSO_4$ + buffer	M-41	2	0.80	1.21	0.32	0.21	0.05	0.02	0.13	21	2.01	4.86	1.29	0.86	0.22	0.07	83.98	8.05	66.58
	M-42	5.5	0.90	9.58	1.76	1.09	0.31	0.09	0.24	34.98	60.66	8.81	1.62	1	0.29	0.08	32.17	55.79	74.66
	M-43	11	1.00	26.52	5.16	1.7	0.47	0.12	0.16	57.31	239.09	8.02	1.56	0.52	0.14	0.04	17.34	72.33	78.02
	M-44	21	1.10	45.5	8.6	1.75	0.27	–	0.09	298.86	619.37	4.67	0.88	0.18	0.03	n.d	30.67	63.56	81.08
	M-45	44	1.23	48.71	4.49	0.05	–	–	0.04	336.84	656.69	4.65	0.43	n.d	n.d	n.d	32.18	62.73	91.54
360 °C C_9 + $MgSO_4$ + buffer	M-46	4	0.80	0.06	0.04	0.03	–	–	–	9.21	0.07	0.63	0.47	0.29	0.06	0.02	97.64	0.78	42.86
	M-47	10	0.90	1.13	0.41	0.25	0.07	0.02	0.12	10.32	1.71	8.02	2.9	1.79	0.54	0.13	73.48	12.16	59.94
	M-48	24	1.00	30.49	8.54	5.09	2.22	0.46	0.31	183.24	311.71	5.62	1.58	0.94	0.41	0.09	33.8	57.5	65.05
	M-49	40	1.10	70.2	22.99	9.18	3.45	1.07	0.35	374.65	666.62	6.11	2	0.8	0.3	0.09	32.62	58.04	65.70
	M-50	72	1.19	73.5	25.78	11.4	4.86	1.73	2.27	485.42	781.79	5.3	1.86	0.82	0.35	0.12	35	56.37	62.72
360 °C MN + $MgSO_4$ + buffer	M-51	10	0.90	0.03	0.01	0.01	–	–	–	5.43	–	0.49	0.13	0.09	n.d	n.d	99.29	n.d	69.01
	M-52	24	1.00	0.02	0.01	–	–	–	–	2.8	–	0.58	0.19	0.12	n.d	n.d	99.11	n.d	65.17
	M-53	40	1.10	0.06	0.01	0.01	–	–	–	12.53	–	0.44	0.08	0.05	n.d	n.d	99.43	n.d	77.19
	M-54	72	1.19	0.06	0.01	–	–	–	–	8.46	1.66	0.57	0.07	0.03	n.d	n.d	83.04	16.29	85.07
	M-55	219	1.40	0.33	0.01	–	–	–	–	74.67	29.66	0.31	0.01	n.d	n.d	n.d	71.33	28.34	96.88

Table 1. Yields and chemical compositions of main products of the thermal cracking simulation experiments.

effects of TSR, experiments were also conducted on nonane (C_9) and methylnaphthalene (MN) at 360 °C following the same procedures. The amount of C_9 and MN added in the experiments were both about 10 mg.

The chemical compositions of gas products were analysed using an Agilent 6890 N gas chromatograph equipped with a PoraPLOT Q column (30 mm × 0.25 mm × 0.25 μm). Helium was used as the carrier gas. The oven temperature was programmed as follows: an initial temperature of 50 °C for 2 min, raised to 180 °C at the rate of 4 °C/min, and held constant at 180 °C for 15 min. Deviation between replicate analyses was less than 1%. The stable carbon isotopic composition was analysed with an Isochrom II GC-IRMS isotope ratio mass spectrometer equipped with a PoraPLOT Q column. Helium was used as the carrier gas. The oven temperature program was started at 50 °C, held for 3 min, raised to 150 °C at a rate of 15 °C/min, and held at 150 °C for 8 min. Each sample was analysed twice with a deviation between the analyses of less than 0.3‰. Stable hydrogen isotope analyses were conducted with a Finningan Delta^{Plus} XL isotope ratio mass spectrometer equipped with a Dim-type column. The oven temperature was programmed as follows: an initial temperature of 40 °C held for 8 min, raised to 110 °C at a rate of 3 °C/min, then held at 110 °C for 2 min. Each analysis was conducted twice, with a deviation between the analyses of less than 4‰. Detailed results are listed in Tables 1 and 2.

Results

Yields of reaction products under different conditions. The yields of all gaseous alkanes produced from thermal cracking of crude oil at 360 °C increased with longer heating time, with CH_4 exhibited the highest yields of 1.00–8.09 ml/g. The yields of H_2S, CO_2 and H_2 also increased with increasing reaction time, but no H_2S was detected in the first 40 h (Table 1). During thermal cracking of a mixture of crude oil, $MgSO_4$, and buffer

Reaction condition	No	Time (h)	$\delta^{13}C$ (‰, VPDB)				$\delta^{2}H$ (‰, VSMOW)		
			CO_2	CH_4	C_2H_6	C_3H_8	CH_4	C_2H_6	C_3H_8
360 °C oil	M-9	10	n.d	−55.8	−37.2	−35.6	−272	−203	−173
	M-10	24	−22.6	−51.3	−35.9	−34.5	−274	−204	−174
	M-11	40	−25.6	−51.5	−36.9	−35.5	−277	−202	−181
	M-12	72	−24.4	−49.1	−35.7	−34.7	−278	−209	−184
	M-13	219	−28.5	−48.4	−36.8	−35.2	−262	−207	−173
350 °C oil + $MgSO_4$ + buffer	M-32	19.5	−20.7	−42.7	−35.9	−33.5	−237	−169	−141
	M-33	42	−23.4	−40.9	−33.6	−29.8	−232	−159	−126
	M-34	79.5	−24.6	−39.2	−31.3	−24.9	−242	−140	−129
	M-35	172	−25.0	−37.0	−21.2	n.d	−216	−101	n.d
360 °C oil + $MgSO_4$ + buffer	M-37	10	−15.7	−41.3	−34.3	−33.1	−226	−174	−136
	M-38	24	−23.1	−36.9	−32.9	−30.4	−227	−153	−114
	M-39	40	−25.1	−36.7	−31.8	−26.5	−224	−134	−105
	M-40	72	−25.6	−36.3	−23.7	n.d	−214	−102	n.d
370 °C oil + $MgSO_4$ + buffer	M-42	5.5	−19.0	−38.8	−34.1	−32.8	−228	−173	−130
	M-43	11	−22.9	−38.1	−33.6	−31.8	−231	−153	−112
	M-44	21	−25.0	−35.0	−29.8	−23.4	−216	−122	−102
	M-45	44	−25.8	−33.7	−21.8	n.d	−199	−106	n.d
360 °C C_9 + $MgSO_4$ + buffer	M-46	4	−2.1	n.d	n.d	n.d	n.d	n.d	n.d
	M-47	10	−10.5	n.d	n.d	n.d	n.d	n.d	n.d
	M-48	24	−23.3	−29.2	−31.6	−30.1	−216	−184	−158
	M-49	40	−24.8	−29.3	−28.5	−26.9	−213	−152	−139
	M-50	72	−25.8	−29.1	−27.6	−26.2	−211	−132	−123
360 °C MN + $MgSO_4$ + buffer	M-51	10	−2.5	n.d	n.d	n.d	n.d	n.d	n.d
	M-52	24	−5.7	n.d	n.d	n.d	n.d	n.d	n.d
	M-53	40	−7.7	n.d	n.d	n.d	n.d	n.d	n.d
	M-54	72	−11.8	n.d	n.d	n.d	n.d	n.d	n.d
	M-55	219	−17.5	n.d	n.d	n.d	n.d	n.d	n.d

Table 2. Carbon and hydrogen isotope compositions of the products of the thermal cracking simulation experiments. Note: n.d. no detection.

at 360 °C (M15–M20), yields of CH_4 and C_2H_6 increased at first and then decreased as the reaction continued. The yield of CH_4 was in the range of 9.94–40.52 ml/g. The yields of C_3H_8, C_4H_{10}, and other heavy gaseous hydrocarbon products gradually decreased with longer heating time. The yield of H_2S increased at first and then decreased in the range of 47.92–378.63 ml/g. The CO_2 yield increased from 41.38 to 190.38 ml/g with time. The yield of H_2 decreased from 0.23 to 0.12 ml/g (Table 1) with increasing heating time. These results suggest that the presence of sulfate significantly increased the yields of H_2S and CO_2.

Compositions of main reaction products under different conditions. During thermal cracking of crude oil at 360 °C, the relative content of alkane gases generally increased with longer heating time, while some decreased as the heating time was increased to 219 h (Table 1). The relative content of CH_4 in the gaseous reaction products ranged from 39.84 to 48.02%, while that of CO_2 exhibited a decreasing trend with increasing heating time. Only trace amounts of H_2S were detected after a heating time of 72 h and 219 h (Table 1). Similarly, it was found that during thermal cracking of a mixture of crude oil, $MgSO_4$, and buffer at 360 °C (M15–M20), the relative content of CH_4 and C_2H_6 first increased and then decreased as the reaction continued. The relative content of CH_4 varied between 6.44% and 13.54%. Concentration of heavy hydrocarbon gases, including C_3H_8 and C_4H_{10}, decreased with longer heating time. The relative content of H_2S and CO_2 remained high during the entire reaction and increased with increased heating time. In all cases, the relative content of H_2S and CO_2 produced from thermal cracking of crude oil increased because of TSR. Thermal cracking (M46–M55) of C_9 and MN in the presence of sulfate also produced high amounts of CO_2 and low amounts of alkane gases (Table 1). To facilitate a comparison with other research and gas geochemical characteristics under actual geological conditions, we modelled the Easy%Ro (Table 1).

Isotopic composition of main reaction products produced under different conditions. Carbon and hydrogen isotopic compositions gaseous reaction products resulting from thermal cracking of various hydrocarbons under a range of experimental conditions are summarised in Table 2 above.

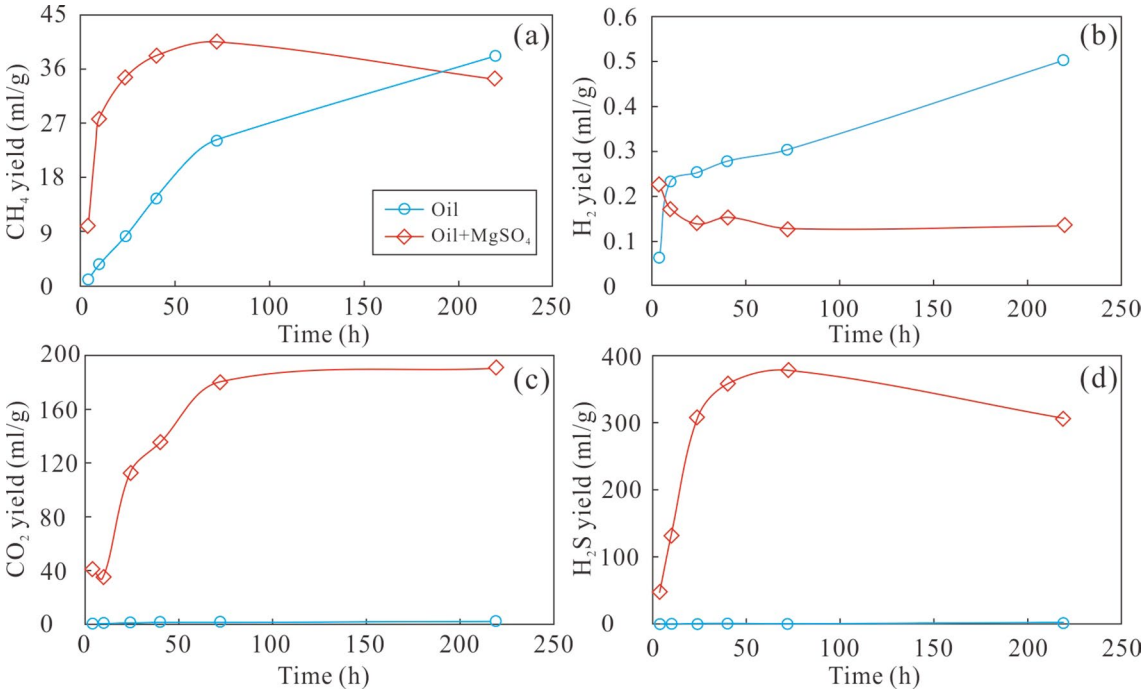

Figure 1. Variations of the yield of major products from thermal cracking of crude oil only (light blue line) and those in the presence of $MgSO_4$ (red line) at the temperature of 360 °C: CH_4 (**a**), H_2 (**b**), CO_2 (**c**), and H_2S (**d**).

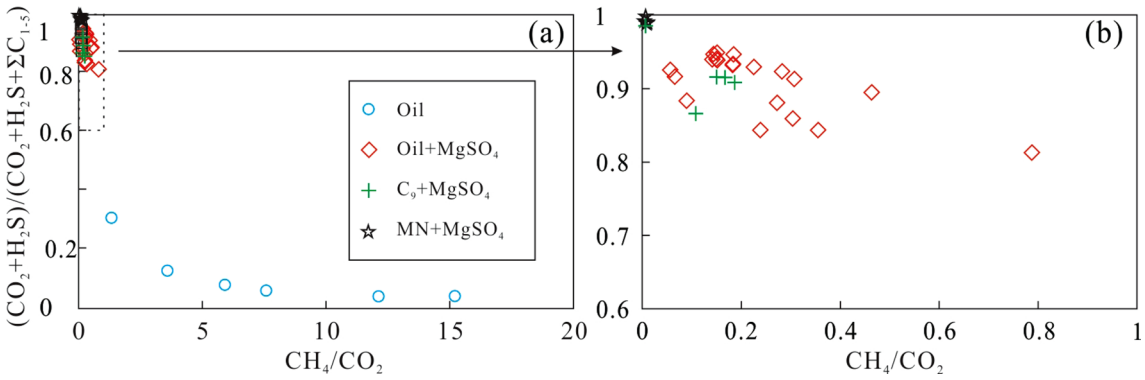

Figure 2. The plot of CH_4/CO_2 versus $(CO_2 + H_2S)/(CO_2 + H_2S + \Sigma C_{1-5})$ during thermal cracking of crude oil and TSR.

Discussion

Yields and relative contents of TRS reaction products. Yield of CH_4, CO_2, and H_2S from direct thermal cracking of crude oil are significantly lower than those resulting from cracking of a crude oil and $MgSO_4$ solution under similar experimental conditions (Table 1). Increased yields of gaseous products might be attributed to the involvement of sulfur in the reaction, which may also trigger TSR[37,38], converting heavier hydrocarbons into CH_4, CO_2, and H_2S[12]. Since the activity energy for alteration of hydrocarbons TSR is lower than that for thermal cracking[38], gas yields from the crude oil and $MgSO_4$ solution is higher than those for thermal cracking of crude oil alone under the same pyrolysis conditions (temperature and time). Compared to the increase of CH_4 yield during thermal cracking of crude oil, the CH_4 yield during thermal cracking of crude oil and $MgSO_4$ rapidly increased in the first 72 h at 360 °C, and then slightly decreased (Fig. 1a), which may be related to the oxidation of methane to H_2S and CO_2 during TSR[12,27]. The H_2 yield from thermal cracking of crude oil gradually increased with time up to 219 h, but the H_2 yield from crude oil and $MgSO_4$ decreased from 0.23 ml/g to 0.15 ml/g until 72 h, and remained almost constant at less than 0.15 ml/g as the reaction continued (Fig. 1b). This observation suggests that TSR may have a very limited effect on H_2 formation during pyrolysis. During the reaction of crude oil and $MgSO_4$, the yield of H_2S and CO_2 increased rapidly before until 72 h (Fig. 1c, d), after which the CO_2 yield remained almost constant as the H_2S yield decreased slightly. Because the presence of a $MgSO_4$ solution introduces sulfur and oxygen into the pyrolysis system, the yield of H_2S and CO_2 increased[12,37]. After 72 h, the yield of CH_4 and H_2S slightly decreased (Fig. 1a, d), indicating that the TSR process consumed

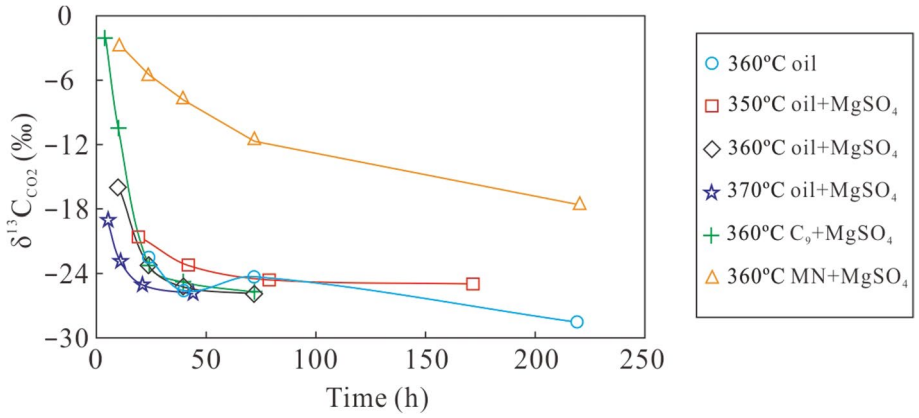

Figure 3. The plot of reaction time versus $\delta^{13}C_{CO2}$ of gaseous products from simulation experiments of different mixtures at various temperatures.

these components to some extent and led to the production of CO_2 and sulfur[27,40,43]. The dryness coefficient (C_1/C_{1-5}) of the gas formed by thermal cracking of crude oil is low, while the dryness coefficient of gas formed during pyrolysis with TSR is higher, accompanied by an increased CH_4 content (Table 1), which further indicates that oxidation of heavy hydrocarbons by TSR will generate CH_4[12,40,43].

Because the source gas of CO_2 and H_2S is produced during the TSR process, the ratios of CH_4/CO_2 and $(CO_2+H_2S)/(CO_2+H_2S+\Sigma C_{1-5})$ were used to investigate variations of the chemical composition of gas altered by TSR. As shown in Fig. 2, ratios of $(CO_2+H_2S)/(CO_2+H_2S+\Sigma C_{1-5})$ sharply decrease with increasing CH_4/CO_2 ratios. The ratio of CH_4/CO_2 for crude oil, C_9, and MN with $MgSO_4$ is less than 1.0, while the ratio of CH_4/CO_2 for thermal cracking of crude oil is above 1.0 (Fig. 2a). In contrast to the ratios of CH_4/CO_2 and $(CO_2+H_2S)/(CO_2+H_2S+\Sigma C_{1-5})$ for crude oil, the same ratios for C_9 and MN with $MgSO_4$ are less than 1.0, and the ratio of $(CO_2+H_2S)/(CO_2+H_2S+\Sigma C_{1-5})$ decreases as the CH_4/CO_2 ratio increases. Compared to the wide range of ratios for pyrolysis of crude oil and $MgSO_4$, the ratio of CH_4/CO_2 and $(CO_2+H_2S)/(CO_2+H_2S+\Sigma C_{1-5})$ for C_9 or MN with $MgSO_4$ shows a smaller range (Fig. 2b). These variations of CH_4/CO_2 and $(CO_2+H_2S)/(CO_2+H_2S+\Sigma C_{1-5})$ caused by thermal cracking of crude oil and different degrees of TSR alteration during pyrolysis are similar to those caused by thermal cracking and TSR alteration of natural gas in gas reservoirs[1,20,21]. Thermal cracking of crude oil produced more CH_4, while TSR increased the yield of CO_2 and H_2S. The content of CH_4 in alkane gas further increased with increased thermal cracking. In contrast, the CO_2 and H_2S contents varied at different stages of TSR. Based on the properties of H_2S-bearing natural gas and previous simulation results[1,6,12,23,40], variations in gas produced by TSR pyrolysis are similar to those of H_2S-bearing natural gas altered by TSR.

Fractionation characteristics of carbon and hydrogen isotopes during TSR. The carbon isotopic composition of produced CO_2 from crude oil, C_9, and MN with $MgSO_4$ at different temperature is negatively correlated with heating time. The $\delta^{13}C_{CO2}$ value gradually decreased from −2.1‰ (C_9, 360 °C, 4 h) to −28.5‰ (crude oil, 360 °C, 219 h) (Table 2, Fig. 3). The carbon isotopic composition of CO_2 from crude oil, C_9, and MN with $MgSO_4$ became significantly lighter over time until about 20 h heating time. After that, the $\delta^{13}C_{CO2}$ value for crude oil and C_9 with $MgSO_4$ remained mostly constant, which is similar to what happens during thermal cracking of crude oil. The decrease of $\delta^{13}C_{CO2}$ values during the first 20 h can be attributed to a greater fractionation of carbon isotopes at the onset of TSR[12]. After 20 h, the carbon isotope fractionation gradually reached a balance between CO_2 and CH_4. Although the $\delta^{13}C_{CO2}$ value for CO_2 produced from MN with $MgSO_4$ decreased with heating time, CO_2 was relatively more enriched in ^{13}C when compared to crude oil, C_9, and $MgSO_4$. In addition to having a heavy carbon isotopic composition, MN was also the most easily oxidised component during TSR. Due to the addition of $MgSO_4$ to MN, MN was quickly oxidised by TSR and converted to gas with CO_2 as the main component. Concentrations of heavy hydrocarbon gases were below the detection limit of the instruments. In summary, the transformation of crude oil, C_9, and MN by TSR converts ^{12}C-rich hydrocarbons to ^{12}C-enriched CO_2, which might be converted to ^{12}C-rich calcite and precipitated in gas reservoirs[9,21].

The $\delta^{13}C$ value of gas produced from crude oil, C_9, and MN with $MgSO_4$ at different temperature and heating times is shown in Fig. 4. With increasing carbon numbers, the carbon isotopes of alkane gas from thermal cracking of crude oil at a pyrolysis temperature of 360 °C became heavier in the order of $\delta^{13}C_1 < \delta^{13}C_2 < \delta^{13}C_3$.

The $\delta^{13}C_1$ values gradually increased over a relatively large range, while both $\delta^{13}C_2$ and $\delta^{13}C_3$ increased in a more narrow range as heating time increased (Fig. 4a). The carbon isotopic composition of alkane gas produced from crude oil and MN with $MgSO_4$ also became heavier with increasing carbon number in the order of $\delta^{13}C_1 < \delta^{13}C_2 < \delta^{13}C_3$. However, at the same temperature, with the addition of $MgSO_4$ solution, $\delta^{13}C_1$ gradually increased in a relatively narrow range, while both $\delta^{13}C_2$ and $\delta^{13}C_3$ showed larger increase as the reaction proceeded (Fig. 4b–d). It is obvious that the $\delta^{13}C_1$ of alkane gas produced in the presence of a $MgSO_4$ solution is higher than that produced during comparative experiments without $MgSO_4$. In a single thermal system, the $\delta^{13}C$ of alkane gas from thermal cracking of crude oil gradually becomes higher with increasing carbon number, and is linearly correlated with the reciprocal of the carbon number (1/n)[44]. The reduction in the variation of $\delta^{13}C_1$

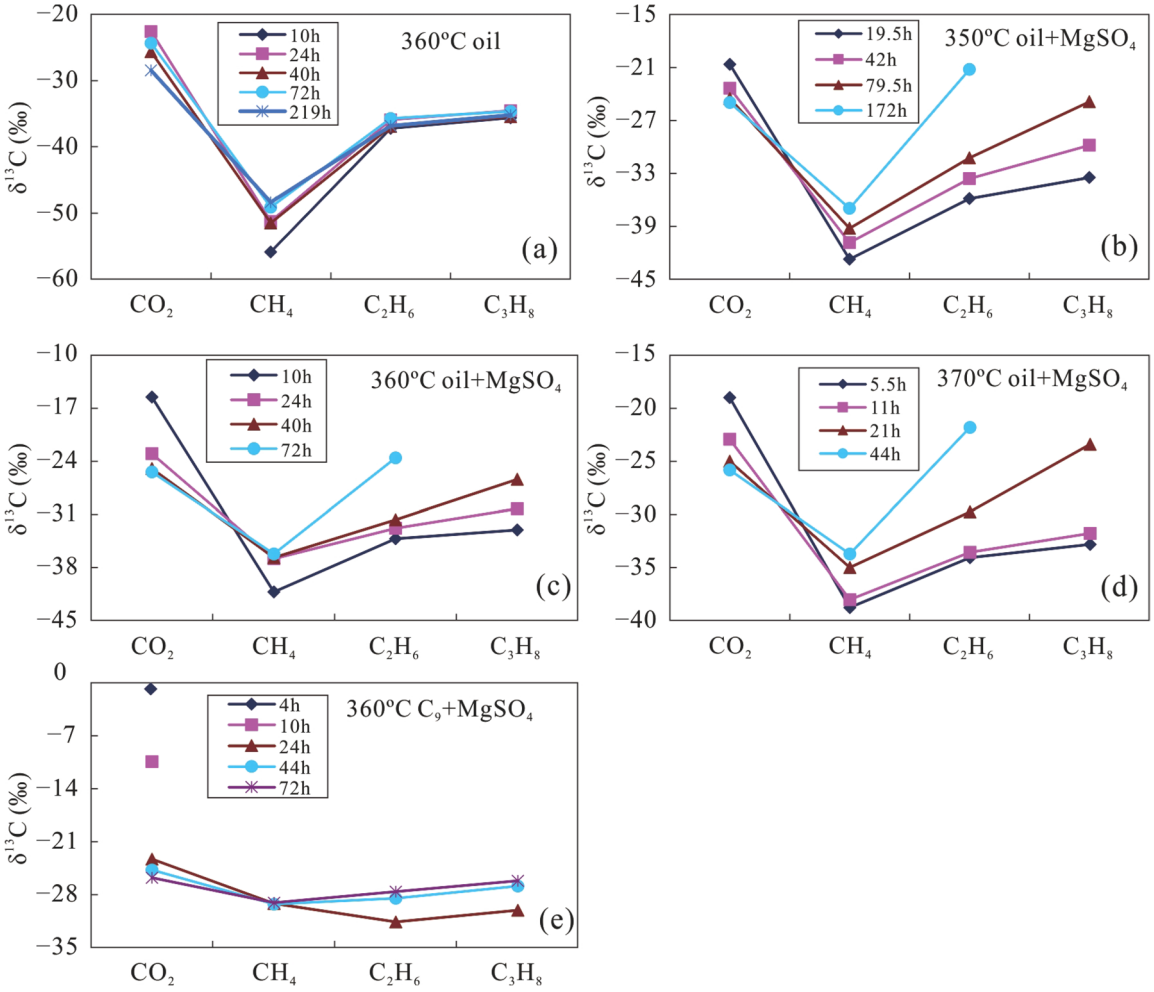

Figure 4. The $\delta^{13}C$ values of products from simulation experiments with crude oil at 360 °C (**a**), a mixture of crude oil and $MgSO_4$ at temperatures of 350 °C (**b**), 360 °C (**c**), 370 °C (**d**), and a mixture of C_9 and $MgSO_4$ at 360 °C (**e**).

values produced by TSR alteration indicates that these hydrocarbons are rapidly oxidised to CH_4 with a $\delta^{13}C_1$ value similar to the source material. The TSR process leads to a ^{13}C increase in CH_4, producing a carbon isotopic composition more similar to that of crude oil (−32.8‰). In contrast, CO_2 becomes gradually enriched in ^{12}C due to equilibrium fractionation of carbon isotopes between CO_2 and CH_4. Overall, the variation of $\delta^{13}C_1$ is significantly smaller in the presence of $MgSO_4$, during TSR of crude oil, similar to that of H_2S-bearing alkane gas in the Sichuan Basin, where natural gas shows a heavy carbon isotopic composition of CH_4[20]. The carbon isotope composition of CO_2formed in the presence of TSR is lighter than that formed in the absence of TSR, because TSR will oxidise a large portion of the hydrocarbons, leading to more intense $\delta^{13}C_{CO2}$ fractionation. Therefore, $\delta^{13}C_{CO2}$ values related to crude oil cracking are relatively heavier, while $\delta^{13}C_{CO2}$ will be relatively enriched in ^{12}C during pyrolysis (with TSR) in the presence of a $MgSO_4$ solution (Table 2).

Our experiments show for the first time that the carbon isotopic composition of gas produced from C_9 with $MgSO_4$ became partially reversed to $\delta^{13}C_1 > \delta^{13}C_2 < \delta^{13}C_3$ after a heating time of 24 h. The CH_4 produced from C_9 with $MgSO_4$ shows an extremely small variation in $\delta^{13}C_1$ values. The variation of $\delta^{13}C_2$ became larger than that of $\delta^{13}C_3$ with longer reaction time (Fig. 4e). This partial reversal of the carbon isotope series of alkane gas is similar to that of H_2S-bearing alkane gas in the Sichuan Basin, Ordos Basin, and other locations[1,16,23]. Therefore, it is likely that the partial reversal of the carbon isotope series of alkane gas in H_2S-bearing natural gas reservoirs happens when light hydrocarbons are altered by TSR. The isotopic composition of reaction products of pyrolysis with MN could not be detected due to the low content of alkane gases.

Figure 5 shows the variation of δ^2H–C_n in alkane gases produced from crude oil at 360 °C, from a mix of crude oil and $MgSO_4$ at 350, 360, and 370 °C, as well as from a mix of C_9 and $MgSO_4$ at 360 °C. Similar to the $\delta^{13}C$ values, the hydrogen isotopic composition of alkane products from crude oil and a mixture of crude oil and $MgSO_4$ became heavier with increasing carbon number under all conditions, i.e. δ^2H–$C_1 < \delta^2H$–$C_2 < \delta^2H$–C_3. The δ^2H–C_1 values gradually increased in a relatively large range, and both δ^2H–C_2 and δ^2H–C_3 increased in a narrower range as heating time increased (Fig. 5a). The δ^2H–C_1 value for a mix of crude oil and $MgSO_4$ gradually increased over time, but in a relatively small range for each temperature. The δ^2H–C_2 and δ^2H–C_3 values also

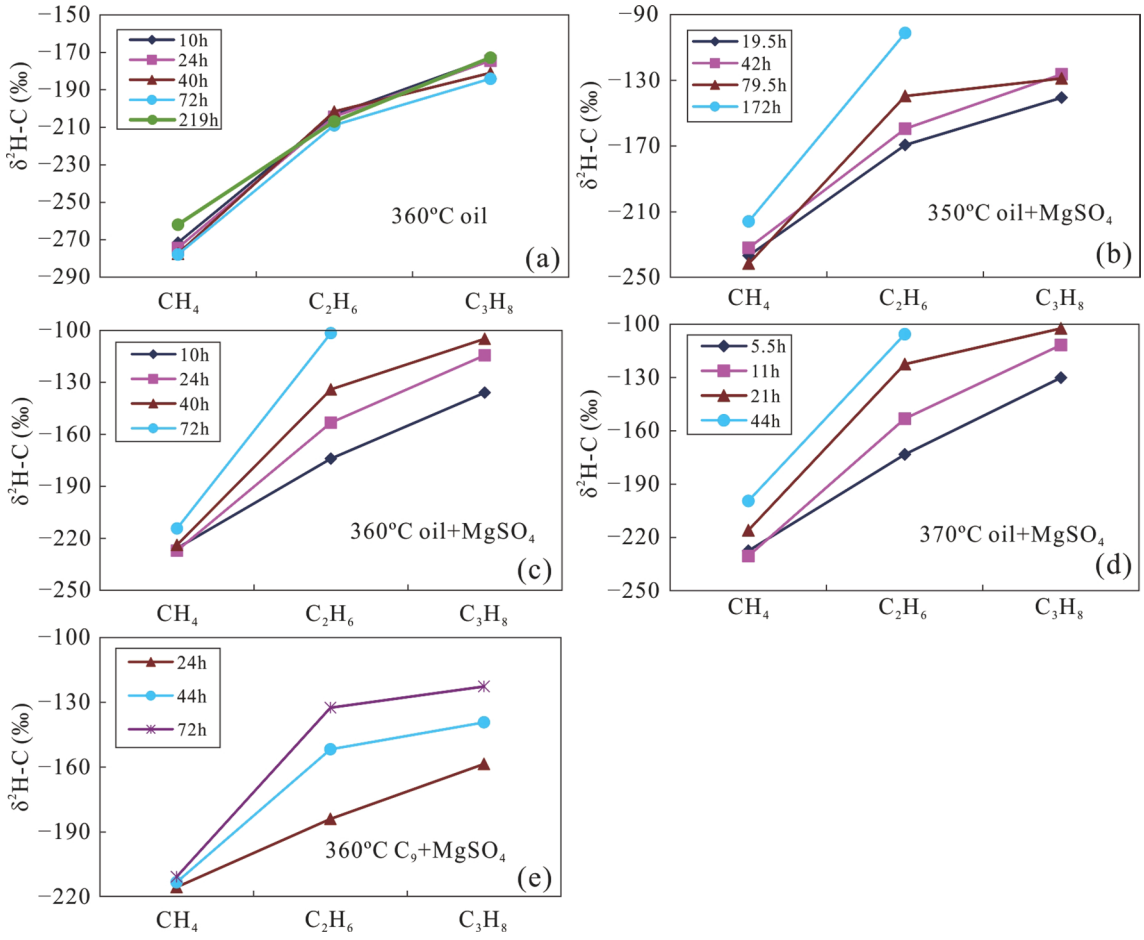

Figure 5. The $\delta^2H–C_n$ of gaseous products from simulation experiments with crude oil at 360 °C (**a**), a mixture of crude oil and $MgSO_4$ at the temperature 350 °C (**b**), 360 °C (**c**), and 370 °C (**d**), as well as a mixture of C_9 and $MgSO_4$ at 360 °C (**e**).

increased with heating time, but in a much larger range compared with that of $\delta^2H–C_1$ (Fig. 5b–d). The variation of $\delta^2H–C_2$ is slightly larger than that of $\delta^2H–C_3$. The $\delta^2H–C_1$ values remained almost constant during the TSR alteration of C_9, while the $\delta^2H–C_2$ values show much larger variations. The $\delta^2H–C_3$ show the largest variations, but a reversed trend of the hydrogen isotopic composition of alkane gas was not observed during pyrolysis (Fig. 5e). These results indicate that the TSR can reduce the variation of $\delta^2H–C_1$, possibly due to the similar hydrogen isotopic composition of the reaction product (C_1 gas) and that of the precursor and/or the involvement of hydrogen derived from water[21]. The $\delta^2H–C_n$ fractionation could not be accurately calculated because of a lack of the hydrogen isotopic composition of H_2 and H_2S. However, TSR of crude oil in the presence of $MgSO_4$ greatly reduced the variation of $\delta^2H–C_1$, which is consistent with the characteristics of H_2S-bearing alkane gas in the reservoirs of the Sichuan Basin, China[45]. In general, hydrogen isotope fractionation during pyrolysis system may be more complicated than fractionation of carbon isotopes, because hydrogen contributes both to formation of alkane gas and H_2, while also providing hydrogen for the formation of H_2S. More importantly, the presence of water may provide an important hydrogen during pyrolysis[21].

These results suggest that TSR can alter both the carbon and hydrogen isotopic composition of gaseous alkane products, and even lead to a reversed trend of the carbon isotope series of CH_4 and C_2H_6 for a mix of C_9 and $MgSO_4$ as the source material. This can result in similar isotopic compositions to those of H_2S-bearing natural gas[45]. Liu et al.[20] investigated carbonate gas systems in the Sichuan Basin of China and found different amounts of acid gases (CO_2 and H_2S) in all marine strata. Both positive carbon isotope series and partially reversed sequence of alkanes were found. The positive carbon isotope series formed during production of sour gases was caused by TSR alteration that preferentially reacted with ^{12}C-bearing heavy hydrocarbons. Therefore, the carbon isotope composition of residual heavy gases became heavier, and the partially-reversed carbon isotope sequence was again converted to be positive series.

In this study, we found that the TSR process played a significant role in the pyrolysis of C_9 and MN with a $MgSO_4$ solution, which lead to production of mainly H_2S and CO_2. TSR is more sensitive to MN, which makes it possible that MN can be completely oxidised into CO_2 and H_2S (Table 1). The smallest variation of both carbon and hydrogen isotopic compositions was observed for CH_4, and was closest to that of the precursor. The heavier carbon isotopic composition of the precursor and C_2H_6 produced from thermal cracking initially led to a reversed

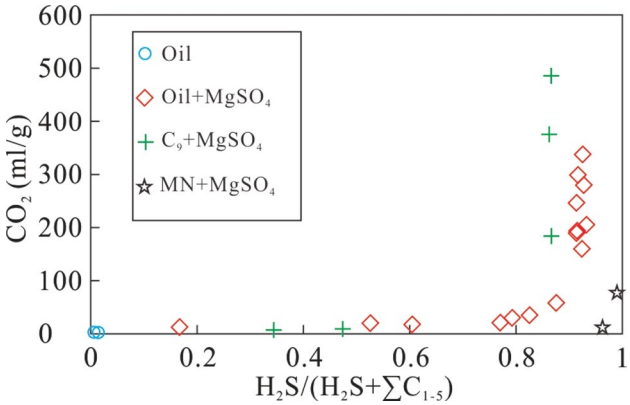

Figure 6. The plot of $H_2S/(H_2S+\Sigma C_{1-5})$ versus CO_2 of simulation products.

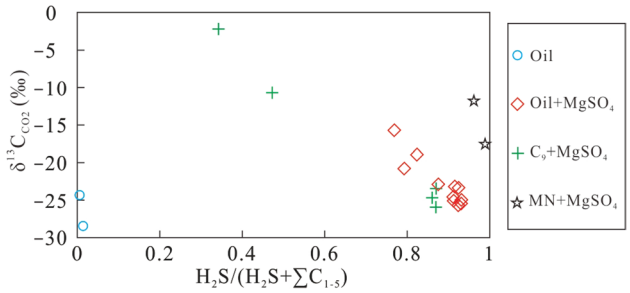

Figure 7. The plot of $H_2S/(H_2S+\Sigma C_{1-5})$ versus $\delta^{13}C_{CO2}$ of simulation products.

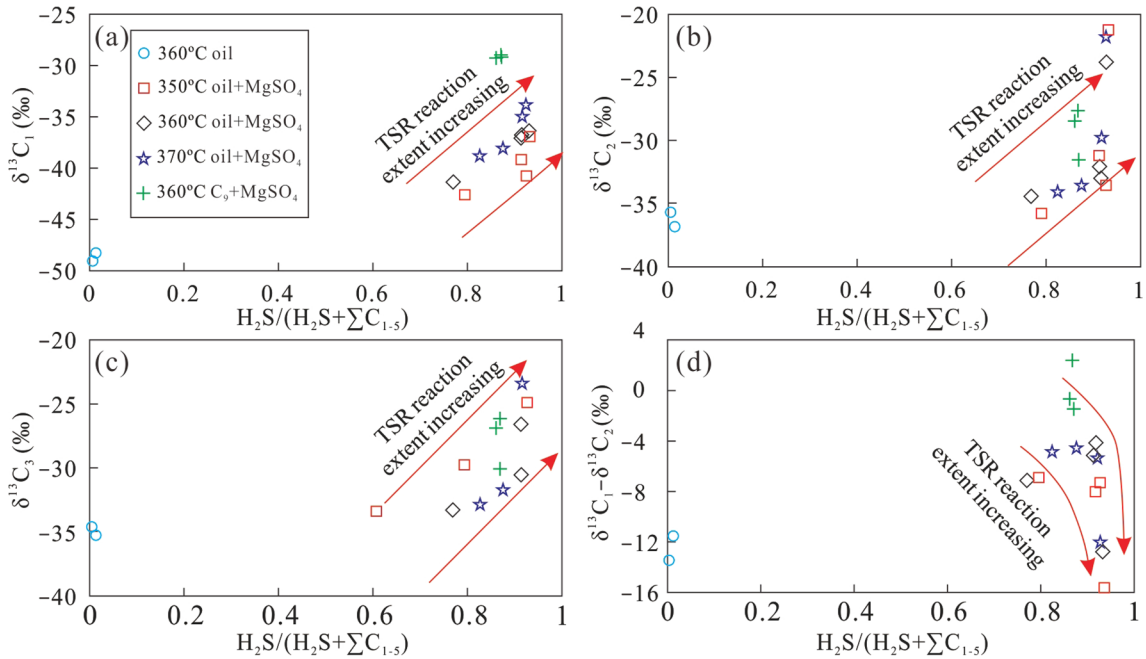

Figure 8. The plot of $H_2S/(H_2S+\Sigma C_{1-5})$ versus $\delta^{13}C_1$ (**a**), $\delta^{13}C_2$ (**b**), $\delta^{13}C_3$ (**c**), $\delta^{13}C_1-\delta^{13}C_2$ (**d**) of alkane gas products from simulation experiments under different conditions.

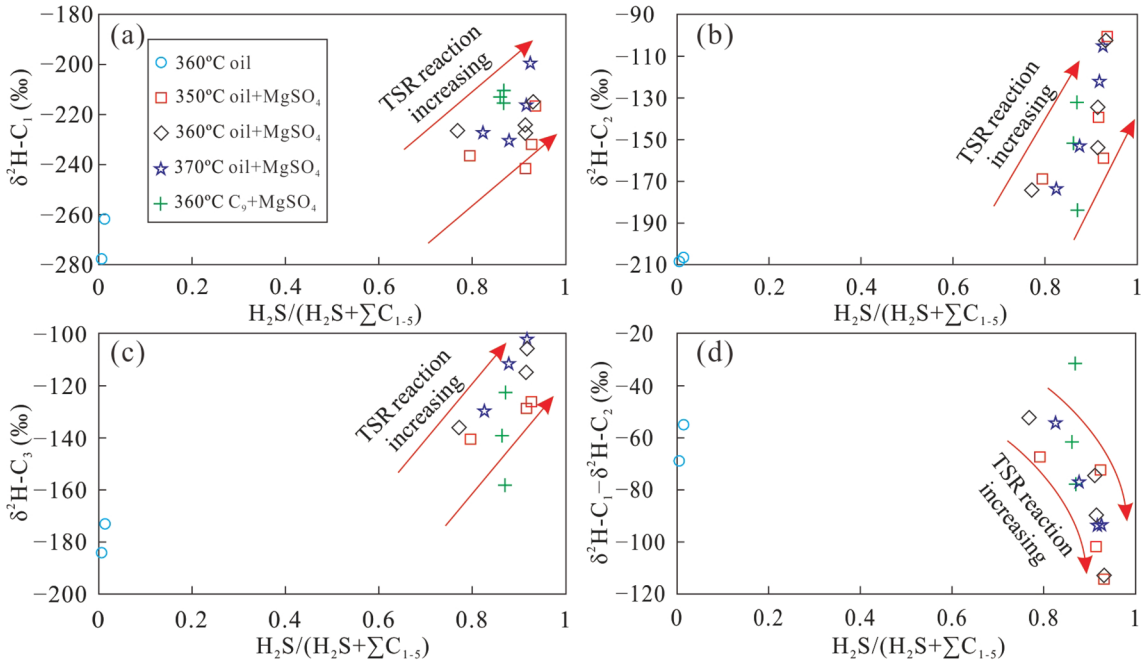

Figure 9. The plot of $H_2S/(H_2S+\Sigma C_{1-5})$ versus $\delta^2H–C_1$ (**a**), $\delta^2H–C_2$ (**b**), $\delta^2H–C_3$ (**c**) and $\delta^2H–C_1–\delta^2H–C_2$ (**d**) of alkane gas products from simulation experiments under different conditions.

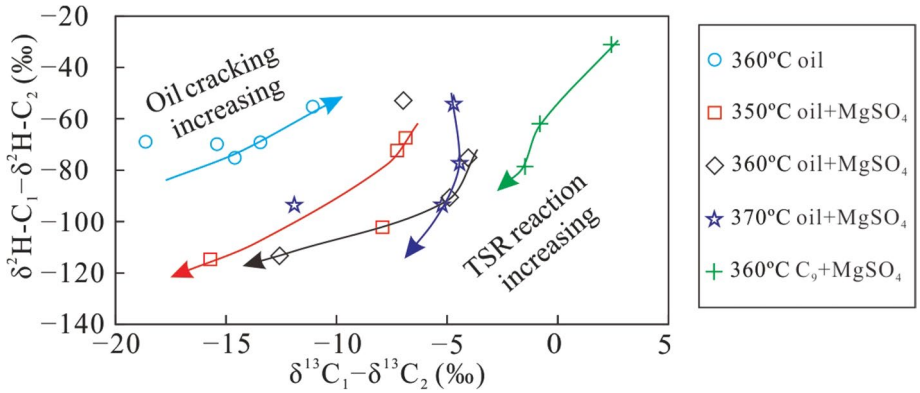

Figure 10. The plot of $\delta^{13}C_1–\delta^{13}C_2$ versus $\delta^2H–C_1–\delta^2H–C_2$ of alkane gas products from simulation experiments under different conditions.

carbon isotope series of the alkane gas (Table 2, M-48). However, the temperature of our experiments (360 °C) was much higher than that in natural geological environments. Therefore, heavy hydrocarbons enriched in ^{12}C tended to become unstable, and were subject to thermal cracking, which led to isotope fractionation. ^{13}C was enriched in the residual heavy hydrocarbons, and the effect of fractionation was larger than that for CH_4 during TSR, changing the carbon isotope sequence back to positive.

Gas souring index (GSI) and carbon and hydrogen isotope fractionation of alkane gas. Because H_2S can be produced during TSR, the gas souring index (GSI), i.e., $H_2S/(H_2S+\Sigma C_{1-5})$, has been used as an indicator for the occurrence and degree of TSR[46]. The variation of the GSI at different stages of TSR can be established by statistical analysis of H_2S-bearing natural gas samples[45]. To reproduce the variation of molecular and isotopic compositions of H_2S-bearing natural gas during TSR, the GSI and carbon and hydrogen isotope fractionation mechanism of alkane gas were studied during pyrolysis at different temperatures with various heating times.

During thermal cracking of crude oil, a very small amount of H_2S with minor CO_2 was produced, indicating that no TSR occurred during direct thermal cracking of crude oil. In contrast, the CO_2 yield gradually increased with a larger GSI (>0.6) for TSR involving a mixture of crude oil and $MgSO_4$ solution, and increased rapidly with further increasing GSI (Fig. 6), which is similar to the relationship between GSI and CO_2 content of H_2S-bearing natural gas[20]. The $\delta^{13}C_{CO2}$ values remained nearly constant but gradually decreased with increasing GSI during thermal cracking due to the presence of TSR (Fig. 7). This phenomenon can be attributed to TSR,

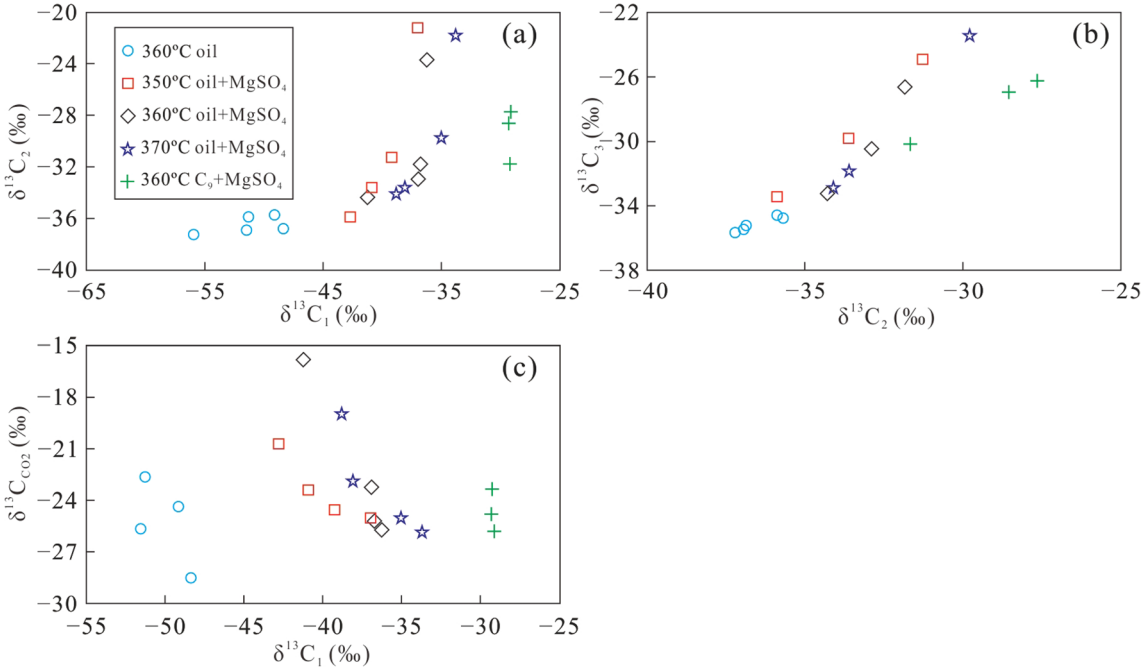

Figure 11. The plot of $\delta^{13}C_1$ versus $\delta^{13}C_2$ (**a**), $\delta^{13}C_2$ and $\delta^{13}C_3$ (**b**) and $\delta^{13}C_1$ and $\delta^{13}C_{CO2}$ (**c**) of alkane gas products from simulation experiments under different conditions.

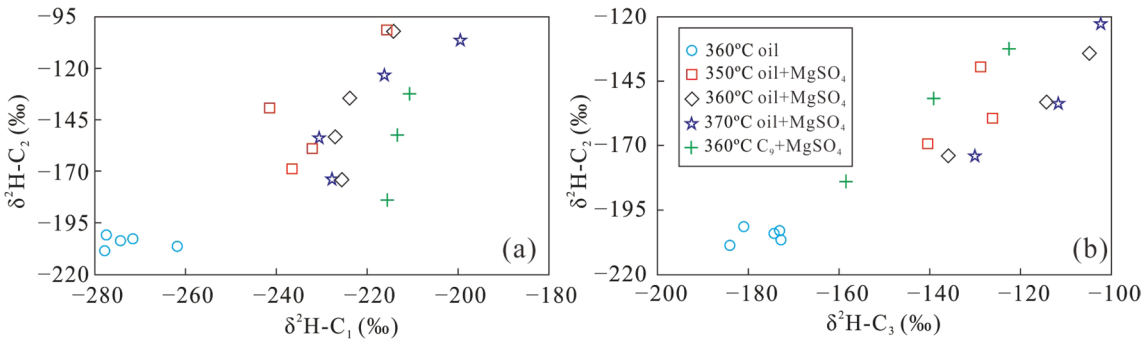

Figure 12. The plot of $\delta^2H–C_1$ versus $\delta^2H–C_2$ (**a**) and $\delta^2H–C_2$ versus $\delta^2H–C_3$ (**b**) of alkane gas products from simulation experiments under different conditions.

which preferentially incorporates ^{12}C from hydrocarbons into CO_2 leading to ^{12}C-enrichment with increasing TSR intensity[44].

Figure 8 shows the relationship between the gas souring index and $\delta^{13}C_1$, $\delta^{13}C_2$, and $\delta^{13}C_3$. The direct thermal cracking of crude oil produced only a small amount of H_2S due to low sulfur content of the crude oil, resulting in a GSI of less than 0.1. The GSI significantly increased with the addition of $MgSO_4$ solution to the crude oil to above 0.6 under different conditions. Meanwhile, the carbon isotopic composition of alkane gas became larger with increasing TSR intensity, i.e., longer reaction time (Fig. 8). The carbon isotopic composition of the alkane gas revealed that the $\delta^{13}C_1$ variation of CH_4 produced in the presence of $MgSO_4$ was much lower than that of C_2H_6. The carbon isotope composition changed more significantly with the increasing GSI and longer heating time. Therefore, during TSR, the variation of $\delta^{13}C_1$ became smaller, compared with that of $\delta^{13}C_2$ and $\delta^{13}C_3$. The $\delta^{13}C_1$–$\delta^{13}C_2$ difference became higher with increasing GSI, which is completely different from that of natural gas formed by direct thermal cracking of crude oil. During thermal cracking of crude oil, the carbon isotope composition of gaseous products gradually becomes more similar with increasing carbon number[45].

The $\delta^2H–C_n$ values of alkane gas show a variation similar to the $\delta^{13}C_n$ values, with increasing GSI during the TSR process. The range of $\delta^2H–C_1$ values is fairly low, while that of $\delta^2H–C_2$ is higher, especially for the TSR of C_9 whose $\delta^2H–C_1$ remained almost constant (Fig. 9). Similar to the carbon isotopic composition, the $\delta^2H–C_1$–$\delta^2H–C_2$ difference increased as the gas souring index became larger, indicating that TSR can lower $\delta^2H–C_1$ values and increase those of $\delta^2H–C_2$, producing an abnormal hydrogen isotope composition of alkane gas, which is only characteristic of thermal cracking of crude oil. Both $\delta^{13}C_1$–$\delta^{13}C_2$ and $\delta^2H–C_1$–$\delta^2H–C_2$ became lower with increasing TSR intensity. However, in the case of oil cracking, $\delta^{13}C_1$–$\delta^{13}C_2$ and $\delta^2H–C_1$–$\delta^2H–C_2$ show the opposite trend with increasing TSR (Fig. 10). This observation may be caused by the small variation of the

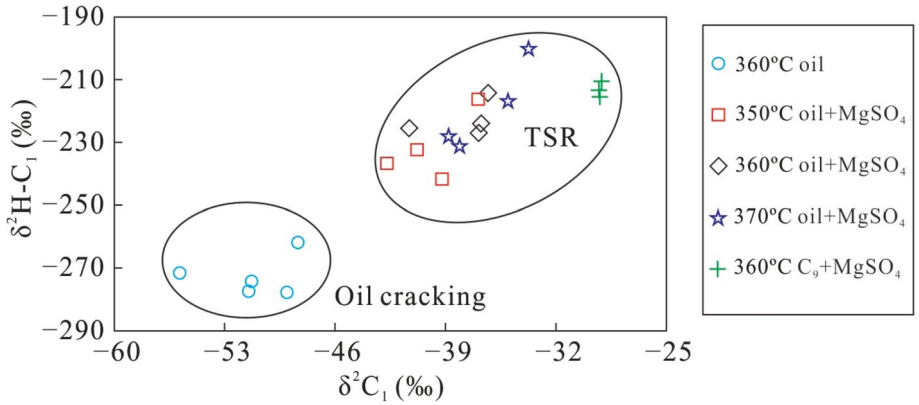

Figure 13. The plot of $\delta^{13}C_1$ versus $\delta^2H–C_1$ of alkane gas products from simulation experiments under different conditions.

$\delta^{13}C_1$ and $\delta^2H–C_1$ produced by TSR, which is similar to the isotopic composition of the precursor. The carbon and hydrogen isotopic composition of C_2H_6 was more heavily affected by the thermal cracking than oxidisation by TSR. Therefore, the variation of its carbon and hydrogen isotope compositions is higher. In addition, the difference in the carbon and hydrogen isotopic composition between CH_4 and C_2H_6 gradually increased with a larger GSI.

Although TSR alteration decreased the variation of both carbon and hydrogen isotope compositions of CH_4, as compared with products from direct thermal cracking of crude oil, $\delta^{13}C_2$ became larger with increasing $\delta^{13}C_1$. The $\delta^{13}C_2$ versus $\delta^{13}C_1$ plot (Fig. 11a), and $\delta^{13}C_2$ versus $\delta^{13}C_3$ plot (Fig. 11b), showed positive correlations, with the latter having a higher correlation. The $\delta^{13}C_1$ and $\delta^{13}C_{CO2}$ values are negatively correlated (Fig. 11c), possibly because the carbon isotopic composition of CO_2 produced by TSR is enriched in ^{12}C[34]. For CH_4, C_2H_6, and C_3H_8, $\delta^2H–C_1$ and $\delta^2H–C_2$ are positively correlated with temperature and heating time. $\delta^2H–C_2$ values increase with increasing $\delta^2H–C_1$ values. The positive correlation between $\delta^2H–C_2$ and $\delta^2H–C_3$ is even more significant (Fig. 12). Based on these results, it can be concluded that the oxidation of hydrocarbons by TSR is accompanied by thermal cracking of crude oil, resulting in distinct patterns among the δ^2H values of alkane gases. Although TSR effect can lead to smaller variations of carbon and hydrogen isotope compositions of CH_4 compared with C_2H_6 and C_3H_8, $\delta^2H–C_1$ values increased with increasing $\delta^{13}C_1$ values (Fig. 13), suggesting that direct thermal cracking of crude oil also produced CH_4. However, the CH_4 produced during pyrolysis of C_9 should be primarily produced by TSR.

All TSR simulation experiments of crude oil, C_9 and MN under different conditions suggest that the TSR alteration produces CH_4 with similar carbon and hydrogen isotopic compositions to those of its precursor and reduced variations of isotopic compositions. The difference between CH_4 and C_2H_6 in carbon isotope and hydrogen isotopic composition increases with increasing TSR intensity, while the carbon and hydrogen isotopic composition of C_2H_6 and C_3H_8 became heavier and shows smaller differences with increasing temperature, similar to the results from thermal cracking of crude oil. The production of alkane gas with similar chemical and isotope compositions to H_2S-bearing natural gas during these experiments, suggest that TSR can alter the carbon and hydrogen isotopic composition of alkane gas[20,21]. In addition, a partially reversed carbon isotope series of alkane gas ($\delta^{13}C_1 > \delta^{13}C_2 < \delta^{13}C_3$) was observed, which further confirms the above conclusion. ^{12}C-enriched CO_2 was mainly produced from the oxidation of hydrocarbons by TSR. However, dissolution of CO_2 and precipitation of carbonate minerals in aqueous fluids can complicate the carbon isotopic composition in the marine carbonate reservoir[45].

Conclusions

Pyrolysis of TSR was carried out using different organic matter (crude oil, nonane and methylnaphthalene), and the characteristics of carbon and hydrogen isotopes, as well as the composition and yields of the reaction products were analysed. The following main conclusions can be drawn:

(1) The carbon and hydrogen isotopic composition of alkane gas generally becomes heavier with increasing carbon number, i.e., $\delta^{13}C_1 < \delta^{13}C_2 < \delta^{13}C_3$ and $\delta^2H–C_1 < \delta^2H–C_2 < \delta^2H–C_3$. At the same temperature, the carbon and hydrogen isotopic composition of CH_4 gradually became larger with longer reaction time. The carbon and hydrogen isotopic composition of C_2H_6 and C_3H_8 also became heavier as the reaction continued, but the variation was significantly larger than that for CH_4. The variation of the carbon and hydrogen isotopic composition of C_2H_6 is higher than that of C_3H_8. Rapid oxidation of source material by TSR produced CH_4 with a small variation in carbon and hydrogen isotopic values, revealing that this process can alter the carbon and hydrogen isotopic composition of CH_4, making it similar to those of the original precursor material.
(2) The partially reversed carbon isotope series observed in alkane gas produced from a mixture of C_9 and $MgSO_4$ indicates that TSR can cause abnormal isotope series of alkane gas in natural gas. As the reaction continued, ^{13}C became enriched in residual heavy hydrocarbon gas, which altered the commonly observed

order of $\delta^{13}C_1 > \delta^{13}C_2$ to a positive carbon isotope series ($\delta^{13}C_1 < \delta^{13}C_2$). For the first time, we confirmed the ability of TSR to alter the isotopic composition of alkanes, causing isotope reversal during TSR pyrolysis.
(3) Under conditions of TSR, hydrogen isotopes of alkane gases form a positive isotope series ($\delta^2H–C_1 < \delta^2H–C_2 < \delta^2H–C_3$). Isotope fractionation is large, especially for ethane and propane, presumably due to the low molecular weight of hydrogen.
(4) During pyrolysis, oil cracking and TSR result in different $\delta^{13}C_1–\delta^{13}C_2$ and $\delta^2H–C_1–\delta^2H–C_2$ evolutionary trends. While $\delta^{13}C_1–\delta^{13}C_2$ and $\delta^2H–C_1–\delta^2H–C_2$ became smaller with increasing intensity of TSR, $\delta^{13}C_1–\delta^{13}C_2$ and $\delta^2H–C_1–\delta^2H–C_2$ became larger with increasing intensity of oil cracking.

Received: 18 January 2020; Accepted: 19 June 2020
Published online: 31 July 2020

References

1. Hao, F. *et al.* Evidence for multiple stages of oil cracking and thermochemical sulfate reduction in the Puguang gas field, Sichuan Basin China. *AAPG Bull.* **92**(5), 611–637. https://doi.org/10.1306/01210807090 (2008).
2. Heydari, E. *et al.* Late burial diagenesis driven by thermal degradation of hydrocarbons and thermochemical sulfate reduction: upper Smackover Carbonates Southeast Mississippi Salt Basin. *AAPG Bull* **72**(2), 197 (1988).
3. Krooss, B. M. *et al.* Origin and distribution of non-hydrocarbon gases. In *Dynamics of complex sedimentary basins–the example of the Central European Basin System* (eds Littke, R. *et al.*) 433–458 (Springer, Berlin, 2008).
4. Machel, H. G. *et al.* Products and distinguishing criteria of bacterial and thermochemical sulfate reduction. *Appl. Geochem.* **10**(4), 373–389. https://doi.org/10.1016/0883-2927(95)00008-8 (1995).
5. Worden, R. H. & Smalley, P. C. H_2S-preducing reactions in deep carbonate gas reservoirs: Khuff Formation Abu Dhabi. *Chem. Geol.* **133**(1–4), 157–171. https://doi.org/10.1016/S0009-2541(96)00074-5 (1996).
6. Worden, R. H. *et al.* The influences of rock fabric and mineralogy upon thermochemical sulphate reduction: Khuff Formation, Abu Dhabi. *J. Sediment. Res.* **70**, 1210–1221. https://doi.org/10.1306/110499701210 (2000).
7. Krouse, H. R. *et al.* Chemical and isotopic evidence of thermochemical sulphate reduction by light hydrocarbon gases in deep carbonate reservoirs. *Nature* **333**(6172), 415–419. https://doi.org/10.1038/333415a0 (1988).
8. Zhang, S. *et al.* Geochemical characteristics of the Zhaolanzhuang sour gas accumulation and thermochemical sulfate reduction in the Jixian Sag of Bohai Bay Basin. *Org. Geochem.* **36**(12), 1717–1730. https://doi.org/10.1016/j.orggeochem.2005.08.015 (2005).
9. Zhu, G. *et al.* Isotopic evidence of TSR origin for natural gas bearing high H_2S contents within the Feixianguan Formation of the northeastern Sichuan Basin, southwestern China. *Sci. China Ser. D-Earth Sci.* **48**(11), 1960–1971. https://doi.org/10.1360/082004-147 (2005).
10. He, K. *et al.* Experimental and theoretical studies on kinetics for thermochemical sulfate reduction of oil, C_{2-5} and methane. *J. Anal. Appl. Pyrol.* **139**, 59–72. https://doi.org/10.1016/j.jaap.2019.01.011 (2019).
11. Yue, C. *et al.* Impact of TSR experimental simulation using two crude oils on the formation of sulfur compounds. *J. Anal. Appl. Pyrol.* **109**, 304–310. https://doi.org/10.1016/j.jaap.2014.06.004 (2014).
12. Pan, C. *et al.* Chemical and carbon isotopic fractionations of gaseous hydrocarbons during abiogenic oxidation. *Earth Planet. Sci. Lett.* **246**(1–2), 70–89. https://doi.org/10.1016/j.epsl.2006.04.013 (2006).
13. Burklé-Vitzthum, V. *et al.* Influence of H_2S on the thermal cracking of alkylbenzenes at high pressure 70 MPa and moderate temperature 583–623 K. *J. Anal. Appl. Pyrol.* **140**, 423–433. https://doi.org/10.1016/j.jaap.2019.04.025 (2019).
14. Nguyen, V. P. *et al.* Thermal reactions between alkanes and H_2S or thiols at high pressure. *J. Anal. Appl. Pyrol.* **103**, 307–319. https://doi.org/10.1016/j.jaap.2012.11.018 (2013).
15. Cai, C. *et al.* Thermochemical sulphate reduction in Cambro-Ordovician carbonates in Central Tarim. *Mar. Pet. Geol.* **18**(6), 729–741. https://doi.org/10.1016/S0264-8172(01)00028-9 (2001).
16. Cai, C. *et al.* Geochemical characteristics and origin of natural gas and thermochemical sulphate reduction in Ordovician carbonates in the Ordos Basin, China. *J. Petrol. Sci. Eng.* **48**(3–4), 209–226. https://doi.org/10.1016/j.petrol.2005.06.007 (2005).
17. Li, J. *et al.* Geochemistry and origin of sour gas accumulations in the northeastern Sichuan Basin SW China. *Org. Geochem.* **36**(12), 1703–1716. https://doi.org/10.1016/j.orggeochem.2005.08.006 (2005).
18. Liu, Q. *et al.* Origin of natural gas from the Ordovician paleo-weathering crust and gas-filling model in Jingbian gas field, Ordos Basin China. *J. Asian Earth Sci.* **35**(1–2), 74–88. https://doi.org/10.1016/j.jseaes.2009.01.005 (2009).
19. Liu, Q. *et al.* Origin of marine sour natural gas and gas-filling model for the Wolonghe Gas Field, Sichuan Basin China. *J. Asian Earth Sci.* **58**, 24–37. https://doi.org/10.1260/0144-5987.32.1.113 (2012).
20. Liu, Q. Y. *et al.* TSR versus non-TSR processes and their impact on gas geochemistry and carbon stable isotopes in Carboniferous, Permian and Lower Triassic marine carbonate gas reservoirs in the Eastern Sichuan Basin China. *Geochim. Cosmochim. Acta* **100**, 96–115. https://doi.org/10.1016/j.gca.2012.09.039 (2013).
21. Liu, Q. Y. *et al.* Thermochemical sulphate reduction (TSR) versus maturation and their effects on hydrogen stable isotopes of very dry alkane gases. *Geochim. Cosmochim. Acta* **137**, 208–220. https://doi.org/10.1016/j.gca.2014.03.013 (2014).
22. Zhu, G. *et al.* The genesis of H_2S in the Weiyuan Gas Field, Sichuan Basin and its evidence. *Chin. Sci. Bull.* **52**(10), 1394–1404. https://doi.org/10.1007/s11434-007-0185-1 (2007).
23. Cai, C. *et al.* Thermochemical sulphate reduction and the generation of hydrogen sulphide and thiols (mercaptans) in Triassic carbonate reservoirs from the Sichuan Basin China. *Chem. Geol.* **202**(1–2), 39–57. https://doi.org/10.1016/S0009-2541(03)00209-2 (2003).
24. Cai, C. *et al.* Methane-dominated thermochemical sulphate reduction in the Triassic Feixianguan Formation East Sichuan Basin, China: towards prediction of fatal H_2S concentrations. *Mar. Pet. Geol.* **21**(10), 1265–1297. https://doi.org/10.1016/j.marpetgeo.2004.09.003 (2004).
25. Cai, C. *et al.* The effect of thermochemical sulfate reduction on formation and isomerization of thiadiamondoids and diamondoids in the Lower Paleozoic petroleum pools of the Tarim Basin NW China. *Org. Geochem.* **101**, 49–62. https://doi.org/10.1016/j.orggeochem.2016.08.006 (2016).
26. Li, K. *et al.* Fluid inclusion and stable isotopic studies of thermochemical sulfate reduction: UPPER PERmian and Lower Triassic gasfields, northeast Sichuan Basin China. *Geochim. Cosmochim. Acta* **246**, 86–108. https://doi.org/10.1016/j.fuel.2019.04.148 (2019).
27. Cai, C. *et al.* Carbon isotope fractionation during methane-dominated TSR in East Sichuan Basin gas fields, China: a review. *Mar. Pet. Geol.* **48**, 100–110. https://doi.org/10.1016/j.marpetgeo.2013.08.006 (2013).
28. Jenden, P. *et al.* Enrichment of nitrogen and ^{13}C of methane in natural gases from the Khuff Formation, Saudi Arabia, caused by thermochemical sulfate reduction. *Org. Geochem.* **82**, 54–68. https://doi.org/10.1016/j.orggeochem.2015.02.008 (2015).
29. Amrani, A. *et al.* The sulfur-isotopic compositions of benzothiophenes and dibenzothiophenes as a proxy for thermochemical sulfate reduction. *Geochim. Cosmochim. Acta* **84**(1), 152–164. https://doi.org/10.1016/j.gca.2012.01.023 (2012).

30. Amrani, A. *et al.* The role of labile sulfur compounds in thermochemical sulfate reduction. *Geochim. Cosmochim. Acta* **72**(12), 2960–2972. https://doi.org/10.1016/j.gca.2008.03.022 (2008).
31. Worden, R. H. *et al.* Gas souring by thermochemical sulfate reduction at 140 °C. *AAPG Bull.* **79**(6), 854–863. https://doi.org/10.1306/8D2B1BCE-171E-11D7-8645000102C1865D (1995).
32. Meshoulam, A. *et al.* Study of thermochemical sulfate reduction mechanism using compound specific sulfur isotope analysis. *Geochim. Cosmochim. Acta* **188**, 73–92. https://doi.org/10.1016/j.gca.2016.05.026 (2016).
33. Xia, X. *et al.* Compositional and stable carbon isotopic fractionation during non-autocatalytic thermochemical sulfate reduction by gaseous hydrocarbons. *Geochim. Cosmochim. Acta* **72**, 4565–4576. https://doi.org/10.1016/j.gca.2014.05.004 (2014).
34. Liu, W. *et al.* An isotope study of the accumulation mechanisms of high-sulfur gas from the Sichuan Basin, southwestern China. *Sci. China Earth Sci.* **59**, 2142–2154. https://doi.org/10.1007/s11430-015-5401-1 (2016).
35. Cross, M. M. *et al.* Thermochemical sulphate reduction (TSR): experimental determination of reaction kinetics and implications of the observed reaction rates for petroleum reservoirs. *Org. Geochem.* **35**(4), 393–404. https://doi.org/10.1016/j.orggeochem.2004.01.005 (2004).
36. Zhang, T. *et al.* Effect of hydrocarbon type on thermochemical sulfate reduction. *Org. Geochem.* **38**(6), 897–910. https://doi.org/10.1016/j.orggeochem.2007.02.004 (2007).
37. Zhang, T. *et al.* Experimental investigation on thermochemical sulfate reduction by H_2S initiation. *Geochim. Cosmochim. Acta* **72**(14), 3518–3530. https://doi.org/10.1016/j.gca.2008.04.036 (2008).
38. Ma, Q. *et al.* Theoretical study on the reactivity of sulfate species with hydrocarbons. *Geochim. Cosmochim. Acta* **72**, 4565–4576. https://doi.org/10.1016/j.gca.2008.05.061 (2008).
39. Zhang, T. *et al.* Kinetics of uncatalyzed thermochemical sulfate reduction by sulfur-free paraffin. *Geochim. Cosmochim. Acta* **96**, 1–17. https://doi.org/10.1016/j.gca.2012.08.010 (2012).
40. Zhao, H. *et al.* Study of thermochemical sulfate reduction of different organic matter: insight from systematic TSR simulation experiments. *Mar. Pet. Geol.* **100**, 434–446. https://doi.org/10.1016/j.marpetgeo.2018.11.009 (2019).
41. Zhang, T. *et al.* Geochemical signatures of thermochemical sulfate reduction in controlled hydrous pyrolysis experiments. *Org. Geochem.* **39**, 308–328. https://doi.org/10.1016/j.orggeochem.2007.12.007 (2008).
42. Schimmelmann, A. *et al.* D/H isotope ratios of kerogen, bitumen, oil, and water in hydrous pyrolysis of source rocks containing kerogen types I, II, IIS, and III. *Geochim. Cosmochim. Acta* **63**, 3751–3766. https://doi.org/10.1016/S0016-7037(99)00221-5 (1999).
43. Cai, C. *et al.* Relative reactivity of saturated hydrocarbons during thermochemical sulfate reduction. *Fuel* **253**(1), 106–113. https://doi.org/10.1016/j.fuel.2019.04.148 (2019).
44. Chung, H. M. *et al.* Origin of gaseous hydrocarbons in subsurface environments: theoretic considerations of carbon isotope distribution. *Chem. Geol.* **71**(1–3), 97–104. https://doi.org/10.1016/0009-2541(88)90108-8 (1988).
45. Liu, Q. *et al.* Origin and carbon isotope fractionation of CO_2 in marine sour gas reservoirs in the Eastern Sichuan Basin. *Org. Geochem.* **74**, 22–32. https://doi.org/10.1016/j.orggeochem.2014.01.012 (2014).
46. Worden, R. H. *et al.* The effects of thermochemical sulfate reduction upon formation water salinity and oxygen isotopes in carbonate gas reservoirs. *Geochim. Cosmochim. Acta* **60**(20), 3925–3931. https://doi.org/10.1016/0016-7037(96)00216-5 (1996).

Acknowledgements

The authors would like to thank the editor Prof. Alon Amrani and the anonymous reviewers for their constructive comments. This work was finished in the State Key Laboratory of Organic Geochemistry, Guangzhou Institute of Geology, Chinese Academy of Science. This research was financially supported by the National Natural Science Foundation of China (Grant Nos: 41625009, 41872122, 41902160), the China Postdoctoral Science Foundation (Grant No. 2019M650967), the National Key Research and Development Plan (Grant No. 2016YFB0600804), and Strategic Priority Research Program of the Chinese Academy of Sciences, China (Grant No. XDA14010404). We acknowledge the support from the Tencent Foundation through the XPLORER PRIZE.

Author contributions

Q.L., W.P. and X.W. wrote the main manuscript text. Q.M., D.Z. and Z.J. reviewed the manuscript, and put forward some constructive suggestions.

Competing interests

The authors declare no competing interests.

Additional information

Correspondence and requests for materials should be addressed to Q.L.

Reprints and permissions information is available at www.nature.com/reprints.

Publisher's note Springer Nature remains neutral with regard to jurisdictional claims in published maps and institutional affiliations.